# Inorganic photosensitizer coupled Gd-based upconversion luminescent nanocomposites for in vivo magnetic resonance imaging and near-infrared-responsive photodynamic therapy in cancers (Postprint)

**Authors:** Zhang, LE, Zeng, LY, Pan, YW, Luo, S, Ren, WZ, Gong, A, Ma, XH, Liang, HZ, Lu, GM, Wu, AG

**Date:** 2017-04-06T00:00:00+00:00

## Abstract

Inorganic photosensitizer coupled Gd-based upconversion luminescent (UCL) nanocomposites have potential application for both magnetic resonance imaging (MRI) and photodynamic therapy (PDT) of cancers using the light stability and biocompatibility of TiO2

## Full Text

## Preamble

**Inorganic Photosensitizer Coupled Gd-Based Upconversion Luminescent Nanocomposites for In Vivo Magnetic Resonance Imaging and Near-Infrared-Responsive Photodynamic Therapy in Cancers**

Yuanwei Pan , Song Luo , Wenzhi Ren , An Gong , Ling' e Zhang , , Leyong Zeng , ,*, Xuehua Ma , Hongze Liang , Guangming Lu , ,**, Aiguo Wu ,*

Key Laboratory of Magnetic Materials and Devices & Division of Functional Materials and Nanodevices, Ningbo Institute of Material Technology and Engineering, Ningbo 315201, PR China

The School of Materials Science and Chemical Engineering, Ningbo University, Ningbo 315211, PR China

Department of Medical Imaging, Jinling Hospital, School of Medicine, Nanjing University, Nanjing 210002, PR China

State Key Laboratory of Analytical Chemistry for Life Science, School of

Chemistry and Chemical Engineering, Nanjing University, Nanjing 210093, PR China

**Article History:** Received 28 September 2014; Accepted 20 December 2014; Available online

**Keywords:** $TiO_2$ inorganic photosensitizer; Gd-based upconversion luminescence; Magnetic resonance imaging; Near-infrared-responsive photodynamic therapy

Inorganic photosensitizer coupled Gd-based upconversion luminescent (UCL) nanocomposites have potential application for both magnetic resonance imaging (MRI) and photodynamic therapy (PDT) of cancers, leveraging the light stability and biocompatibility of $TiO_2$ inorganic photosensitizer. However, $TiO_2$ inorganic photosensitizer can only be excited by ultraviolet (UV) light, which is harmful and has weak tissue penetration. In this work, folic acid (FA)-targeted $NaGdF_4$:Yb/Tm@$SiO_2$@TiO$_{2}$ nanocomposites (FA-Gd-Si-Ti NPs) were constructed and synthesized for both in vivo MRI and near-infrared (NIR)-responsive inorganic PDT, wherein the $TiO_2$ component could be excited by NIR light due to the UCL performance of the $NaGdF_4$:Yb/Tm component converting NIR to UV light. The results showed that the as-prepared FA-Gd-Si-Ti NPs had good biocompatibility in vitro and in vivo. Moreover, MR studies indicated that FA-Gd-Si-Ti NPs were effective $T_1$-weighted MRI contrast agents with high longitudinal relaxivity ($r_1$) of 4.53 $mM^{-1}s^{-1}$. In vivo MRI of nude mice showed "bright" signal in MCF-7 tumors. Under irradiation of a 980 nm laser at a power density of 0.6 $W/cm^2$ for 20 min, the viability of HeLa and MCF-7 cells incubated with FA-Gd-Si-Ti NPs decreased from about 90% to 35% and 31%, respectively. Furthermore, in vivo PDT of MCF-7 tumor-bearing nude mice showed that the tumor inhibition ratio reached up to 88.6% after 2-week treatment compared with the control group. Based on the deep penetration of NIR light and the good biocompatibility of $TiO_2$ inorganic photosensitizer, the as-prepared FA-Gd-Si-Ti NPs could have potential applications in both MRI and NIR-responsive PDT of cancers in deep tissues.

## 1. Introduction

Magnetic resonance imaging (MRI) and photodynamic therapy (PDT) have potential applications in early diagnosis, therapy, and prognosis assessment of cancers. Particularly, PDT is considered very promising for noninvasive treatment of malignant tumors due to its high sensitivity and selectivity [1–4]. Under an external light source, photosensitizers can be excited to induce cytotoxic reactive oxygen species that aggressively destroy cancer cells. However, single photosensitizers typically have poor tumor localization ability and cannot remain in the body for long periods, limiting therapeutic accuracy and efficiency to some extent [5,6].

In recent years, photosensitizers combined with nanomaterials as multifunctional PDT agents have attracted great attention for simultaneous imaging

and therapy, such as Au nanorods@mSiO$_2$-porphyrin for two-photon imaging and PDT [7], NaYF$_4$:Yb/Er-ZnPc for fluorescence imaging and PDT [8], NaYF$_4$:Yb,Er/NaGdF$_4$-Ce6 for dual-modal imaging and PDT [9], and others [10–12]. Because of the enhanced permeability and retention effect, TiO$_2$ inorganic photosensitizer coupled with Gd-based upconversion luminescent (UCL) nanoparticles could be used for T$_1$-weighted MRI and NIR-responsive PDT of cancers, which is interesting for early diagnosis, therapy, and prognosis assessment of cancers.

Herein, folic acid (FA)-targeted NaGdF$_4$:Yb/Tm@SiO$_2$@TiO$_{2}$ nanocomposites were designed and synthesized for both T$_1$-weighted MRI and inorganic PDT under NIR light excitation. In this structure, the NaGdF$_4$:Yb/Tm component serves as a T$_1$-weighted MRI contrast agent and the TiO$_2$ component serves as a PDT agent. Due to the UCL performance of NaGdF$_4$:Yb/Tm converting NIR light into UV light, TiO$_2$ can be excited by NIR light for PDT in deep tissues. The detailed schematic illustration of FA-targeted NaGdF$_4$:Yb/Tm@SiO$_2$@TiO$_{2}$ nanocomposites for MRI and near-infrared-responsive PDT is shown in Fig. 1 FIGURE:1.

## 2.1. Materials

Rare-earth oxides including gadolinium oxide (Gd$_2$O$_3$, 99.9%), ytterbium oxide (Yb$_2$O$_3$, 99.9%), thulium oxide (Tm$_2$O$_3$, 99.99%), polyvinylpyrrolidone (PVP, K29-32), ammonium fluoride (NH$_4$F, 98%), ammonium hydroxide (NH$_3$$H2O, 25e28%), Tetraethyl orthosilicate (TEOS, 99.9%), titanium butoxide (TBOT, (cid:3)99.0%), (3- aminopropyl)triethoxysilane (APTES, 99%), and dimethyl sulfoxide (DMSO, analyt- ical grade) were purchased from Aladdin Industrial Inc. (Shanghai, China). Sodium chloride (NaCl, analytical grade), hydrochloric acid (HCl, analytical grade), nitric acid (HNO3, analytical grade), ethylene glycol (EG, analytical grade), absolute ethanol (analytical grade), folic acid (FA), 1-ethyl-3-(3-dimethylaminopropyl) carbodiimide hydrochloride (EDAC), N-hydroxysuccinimide (NHS), and 3-(4,5-di-methylthiazol- 2-yl)-2,5-diphenyltetrazolium bromide (MTT) were purchased from Sinopharm Chemical Reagent Co., Ltd. (Shanghai, China). Dulbecco' s modified Eagle' s medium (DMEM), fetal bovine serum (FBS), penicillin and streptomycin were purchased from Invitrogen (USA). All reagents were used as received without further purification.

Milli-Q water (18.2 MU cm) was used in all experiments. (EPR) effect, and with the guidance of imaging, the accuracy and efficiency of PDT were greatly promoted.

However, organic molecules usually used as photosensitizers in PDT [1,9e14], which have some drawbacks, for example easy light bleaching, quick circulation, poor stability even in the absence of light, and so on. TiO2 nanoparticles were well known as inorganic photosensitizers widely used for photocatalytic degradation in environment [15e19], but they also could be applied in

PDT [20e23]. Under the excitation of ultraviolet (UV) light, TiO2 nano- particles could produce reactive oxygen species, such as hydroxyl (cid:1) radicals (OH), $superoxideanion(O\_\{2\}\$^{-})$, hydrogen peroxide ($H_2O_2$) and singlet oxygen ($^1O_2$) would oxidize proteins and lipids in the cell membrane and cellular components, finally causing cell death through both apoptosis and necrosis [23,24]. Specifically, inorganic $TiO_2$ nanoparticles have good light stability, good biocompatibility, and long retention time in the body, making them favorable for biomedical applications. Previously, our research group synthesized Janus $Fe_3O_4$-$TiO_2$ nanocomposites for $T_2$-weighted MRI and inorganic PDT under UV light [25].

However, $TiO_2$ inorganic photosensitizer can only be excited by UV light for PDT, which has weak penetration ability and can cause additional damage to normal tissues. Therefore, it is a crucial challenge to explore a noninvasive light source to trigger $TiO_2$ inorganic photosensitizer for PDT of cancers in deep tissues.

It is well known that near-infrared (NIR) light has deep penetration in the body and is noninvasive to tissues and organs [26,27]. $NaGdF_4$ nanoparticles doped with lanthanide, such as Yb/Er or Yb/Tm, can convert NIR light into visible or UV light [28–30]. Moreover, $NaGdF_4$ nanoparticles have been widely developed as $T_1$-weighted MRI contrast agents due to their excellent biocompatibility compared with Gd-based chelates [31–35]. Therefore, $TiO_2$ inorganic photosensitizer coupled with Gd-based upconversion luminescent nanoparticles could be used for $T_1$-weighted MRI and NIR-responsive PDT of cancers.

## 2.2. Synthesis of FA-Targeted $NaGdF_4$:Yb/Tm@$SiO_2$@TiO$_\{2\}$ Nanocomposites

### 2.2.1. Synthesis of $NaGdF_4$:Yb/Tm@$SiO_2$@TiO$_\{2\}$ NPs (Gd-Si-Ti NPs)

First, $NaGdF_4$:Yb/Tm NPs were prepared following a previously reported method [36]. PVP (10 mg) and NaCl (1 mmol) were added to $RECl_3$ (RE = Gd, Yb or Tm; Gd:Yb:Tm = 0.795 mmol:0.2 mmol:0.005 mmol) dissolved in 10 mL EG, and heated to 80 (cid:4)C to form a homogeneous solution. Then $NH_4F$ (4 mmol) in 10 mL EG solution at 80 (cid:4)C was added dropwise to the $RECl_3$ solution under constant stirring at room temperature until a transparent solution formed. Finally, the mixed solution was transferred to an autoclave and maintained at 180 (cid:4)C for 12 h. The resultant $NaGdF_4$:Yb/Tm NPs were collected by centrifugation (10,000 rpm for 10 min) and washed with Milli-Q water and ethanol three times each.

Second, $NaGdF_4$:Yb/Tm@$SiO_2$ NPs (Gd-Si NPs) were prepared. The $SiO_2$ shell was coated onto $NaGdF_4$:Yb/Tm NPs through the versatile Stöber method as follows: $NaGdF_4$:Yb/Tm UCNPs (15 mg) were redispersed into a mixture containing absolute ethanol (28 mL), Milli-Q water (7 mL) and ammonium

hydroxide (0.7 mL) under ultrasound for 10 min. Afterwards, 25 mL of TEOS (in 3 mL absolute ethanol) was added dropwise over 10 min under continuous stirring. The reaction was kept for 6 h at room temperature and the resultant Gd-Si NPs were collected by centrifugation (10,000 rpm for 10 min) and washed with Milli-Q water and ethanol three times each.

Third, Gd-Si-Ti NPs were finally prepared. 7 mL of TBOT was added to 15 mL absolute ethanol containing 15 mg Gd-Si NPs. Then 1.5 mL of $HNO_3$ solution (50 mM) was immediately added to the above solution. Subsequently, the solution was transferred to an autoclave and maintained at 180 (cid:4)C for 10 h. After the autoclave cooled to room temperature naturally, the resultant Gd-Si-Ti NPs were collected by centrifugation (10,000 rpm for 10 min) and washed with Milli-Q water and ethanol three times, and finally redispersed in 5 mL absolute ethanol.

### 2.2.2. Amino Modification and FA Conjugation

For amino modification on the surface of Gd-Si-Ti NPs, 20 mL absolute ethanol and 1.5 mL Milli-Q water were added to the above Gd-Si-Ti NPs solution, and 15 mL of APTES (in 5 mL absolute ethanol) was added dropwise. The reaction was kept at 50 (cid:4)C under continuous stirring for 3 h. Finally, the resultant nanoparticles ($NH_2$-Gd-Si-Ti NPs) were collected by centrifugation (10,000 rpm for 10 min) and washed with Milli-Q water and ethanol three times each.

For FA conjugation, 12 mg FA was dispersed in 12 mL PBS (pH = 7.4), and the solution was stored in a refrigerator at 4 (cid:4)C for 20 min. Afterwards, EDAC (10 mg) and NHS (6 mg) were quickly added to the cooled FA solution, and the mixed solution was stirred at room temperature for 8 h to activate FA. After that, 1 mL of the activated FA solution (1 mg/mL in PBS) was added to 12 mL of $NH_2$-Gd-Si-Ti NPs solution (1.0 mg/mL in Milli-Q water). The reaction was kept at room temperature under continuous stirring for 16 h. The resultant nanoparticles (FA-Gd-Si-Ti NPs) were collected by centrifugation (12,000 rpm for 20 min).

## 2.3. Characterization

Transmission electron microscopy (TEM) and high-resolution TEM (HRTEM) images were obtained on a JEOL-2100 transmission electron microscope operating at 200 kV. Powder X-ray diffraction (XRD) measurements were performed on a D8 Focus diffractometer (Bruker) using Cu-K$\alpha$ radiation, operating at 40 kV and 40 mA. Dynamic light scattering (DLS) and zeta-potential experiments were conducted on a Zetasizer Nanoseries (Nano-ZS, Malvern Instruments). UCL spectra were recorded on an F-4600 fluorescence spectrophotometer (Hitachi, Japan), using an external 0–2 W adjustable 980 nm semiconductor laser (HI-Tech Optoelectronics Co., Ltd.) as the excitation source. Inductively coupled plasma optical emission spectrometry (ICP-OES) was performed with an Optima 2100 instrument from Perkin Elmer.

## 2.4. Cell Culture, Cytotoxicity and Cellular Uptake

Human breast cancer cell line (MCF-7 cells) and human cervical carcinoma cell line (HeLa cells) were cultured in complete DMEM medium supplemented with 10% fetal bovine serum (FBS), 100 units/mL penicillin and 100 mg/mL streptomycin at 37 (cid:4)C in a humidified atmosphere of 5% $CO_2$.

To evaluate the biocompatibility of the nanomaterials, MTT assay was performed on MCF-7 and HeLa cells. Briefly, 100 mL of cells (MCF-7 and HeLa) were seeded in a 96-well plate at a density of 1 (cid:5) $10^5$ cells/mL and incubated for 24 h. Serial concentrations of the nanoparticles ($NaGdF_4$:Yb/Tm, Gd-Si-Ti NPs, and FA-Gd-Si-Ti NPs) in 100 mL culture medium were added and incubated for another 24 h. The final concentrations of the nanoparticles were 100, 200, 300, 400, and 500 mg/mL, respectively. The absorbance of the suspension was recorded by a microplate reader (iMark 168-1130, Bio-rad, USA) at a wavelength of 550 nm.

Bio-TEM was performed to investigate the cellular uptake of FA-Gd-Si-Ti NPs. Briefly, MCF-7 and HeLa cells were incubated with FA-Gd-Si-Ti NPs at 500 mg/mL for 12 h. Subsequently, the cells were washed twice with PBS and detached by trypsin-EDTA. The obtained cells were washed with PBS and collected by centrifugation at 1000 rpm for 5 min. Bio-TEM images were obtained on a JEOL JEM-1011 transmission electron microscope operating at 100 kV.

**In vitro MRI test:** The in vitro relaxation times ($T_1$, $T_2$) of FA-Gd-Si-Ti NPs were measured on a 0.47 T Micro MR instrument at a frequency of 23.318 MHz (Niumag, Shanghai, China). Dilutions of FA-Gd-Si-Ti NPs samples in Milli-Q water with various Gd concentrations (0, 0.2, 0.4, 0.6, 0.8, and 1.0 mM) were placed in a tube holder for relaxivity measurements. Values of $T_1$ and $T_2$ were measured, and longitudinal ($r_1$) and transverse ($r_2$) relaxivities were calculated from the slope of inverse relaxation times ($1/T_1$ and $1/T_2$) plotted against different Gd concentrations.

MRI experiments of FA-Gd-Si-Ti NPs and cells incubated with FA-Gd-Si-Ti NPs were conducted on a 3.0 T clinical MR instrument (Siemens Trio). FA-Gd-Si-Ti NPs with various Gd concentrations (0, 0.2, 0.4, 0.6, 0.8, and 1.0 mM) were dispersed in 1% gelose solution. For MRI of MCF-7 and HeLa cells incubated with FA-Gd-Si-Ti NPs, 1 (cid:5) $10^5$ cells were seeded in each 1 cm-culture dish for 24 h. After incubation with FA-Gd-Si-Ti NPs at Gd concentrations from 0 to 1.0 mM for another 24 h, the cells were washed with PBS, collected by centrifugation at 1000 rpm for 5 min, and finally redispersed in 1% gelose solution for MR imaging.

**In vitro PDT for MCF-7 and HeLa cells:** First, 100 mL of cells (MCF-7 and HeLa) were seeded in a 96-well plate at a density of 1 (cid:5) $10^5$ cells/mL and incubated for 24 h at 37 (cid:4)C in 5% $CO_2$. Then 100 mL of FA-Gd-Si-Ti NPs (1000 mg/mL, in culture medium) and $NaGdF_4$:Yb/Tm NPs (468 mg/mL, in culture medium) were added to each well. After 4 h, the cells were

irradiated by NIR light using a 980 nm semiconductor laser at a power density of 0.6 W/cm$^2$ for exposure times from 0 to 20 min. To avoid heat damage to cells, the 980 nm laser treatment was applied with 5 min intervals for every 5 min of laser irradiation. After irradiation, the cells were incubated for another 20 h. Finally, cell viability was measured by MTT assay.

Alternatively, dye molecules calcein acetoxymethyl ester (CAM) and propidium iodide (PI) were used to stain cells to investigate viability, allowing intuitive distinction between live and dead cells [25]. 0.5 mL of cells was seeded in a 48-well plate at densities of 4.5 (cid:5) $10^4$ and 2.5 (cid:5) $10^4$ cells per well for HeLa and MCF-7 cells, respectively, and incubated for 24 h. Then 0.5 mL of FA-Gd-Si-Ti NPs and $NaGdF_4$:Yb/Tm NPs (1000 mg/mL, in culture medium) were added to each well and incubated for 4 h. The cells were then irradiated by a 980 nm laser at 0.6 W/cm$^2$ for 0 and 20 min, and incubated for another 20 h. The 980 nm laser was applied with 5 min intervals for every 5 min of irradiation. Finally, the culture medium was removed, and CAM/PI mixed solution (in 0.25 mL PBS) was added to each well for staining. The green and red fluorescent emissions of CAM and PI were observed under an inverted fluorescence microscope (Leica, DMI3000).

**In vivo toxicity and tumor model:** Female Balb/c (nu/nu) nude mice (18-20 g, 4-6 weeks old) were used in this work. All experimental protocols involving animals were approved by the Institutional Animal Care and Use Committee of Jinling Hospital, and all mice received humane care in compliance with the Guide for the Care and Use of Laboratory Animals. Moreover, the experiments were performed in the Animal Centre of Jinling Hospital.

For in vivo toxicity, 12 healthy nude mice were randomly divided into two groups (n = 6 each) and injected with 100 mL of FA-Gd-Si-Ti NPs (5 mg/mL) and 100 mL PBS as control every four days via tail vein. Behavior and body weight were observed for 14 days. To further verify in vivo toxicity, mice were sacrificed on day 14 and major organs including heart, liver, spleen, lung, kidney and intestine were stained with Hematoxylin and Eosin (H&E) and examined by optical microscope (Leica, DMI3000).

A tumor model of human breast cancers was established by subcutaneous injection of MCF-7 cells. Briefly, MCF-7 cells were diluted with PBS and injected subcutaneously into each mouse at the back with approximately 1 (cid:5) $10^7$ cells. After two weeks, tumors grew to about 50-100 mm$^3$.

**In vivo MRI and PDT:** $T_1$ and $T_2$-weighted MRI of MCF-7 tumor-bearing nude mice were performed by intratumoral injection of FA-Gd-Si-Ti NPs solution (500 mg/mL) in PBS at the tumor site after 2 h. MRI was also performed before injection as control.

For in vivo PDT, MCF-7 tumor-bearing mice were randomly divided into four groups (n = 6 each): (1) group 1: only intratumoral injection of 100 mL PBS (control group); (2) group 2: intratumoral injection of 100 mL PBS and NIR irradiation; (3) group 3: only intratumoral injection of 100 mL FA-Gd-Si-Ti

NPs (500 mg/mL, in PBS); (4) group 4: intratumoral injection of 100 mL FA-Gd-Si-Ti NPs (500 mg/mL, in PBS) and NIR irradiation. For groups 2 and 4, tumors were irradiated twice by a 980 nm laser at 4 h and 24 h after injecting PBS or FA-Gd-Si-Ti NPs. The power density was 0.6 W/cm$^2$ and irradiation time was 20 min. To avoid heat damage to tissues, the 980 nm laser treatment was applied with 5 min intervals for every 5 min of irradiation. After treatment, tumor volume was calculated as length × (width)$^2$ × 1/2 with a caliper, and body weight of each mouse was monitored every two days over two weeks.

## 3.1. Synthesis and Characterization of FA-Gd-Si-Ti NPs

Fig. 1(b)-(d) shows TEM images of the as-prepared $NaGdF_4$:Yb/Tm, Gd-Si and Gd-Si-Ti NPs, respectively. As shown in Fig. 1(b), $NaGdF_4$:Yb/Tm NPs were nearly spherical or rodlike with sizes of about 50–80 nm. The HRTEM image inset in Fig. 1(b) indicated that the distance between lattice fringes was 0.302 nm, corresponding to the d-spacing of the (110) lattice plane in the hexagonal $NaGdF_4$ structure. Using the Stöber method, a silica layer about 20 nm thick was coated onto $NaGdF_4$:Yb/Tm to form Gd-Si NPs, as shown in Fig. 1(c). Further, many $TiO_2$ crystals with sizes of 3–5 nm were deposited onto Gd-Si NPs, finally synthesizing Gd-Si-Ti NPs, as shown in Fig. 1(d).

The crystal structure of the as-prepared nanoparticles was further characterized by XRD analysis. As shown in Fig. 2 FIGURE:2, all diffraction peaks of $NaGdF_4$:Yb/Tm NPs agreed well with pure hexagonal $NaGdF_4$ (JCPDS NO. 27-0699). After coating with $SiO_2$ and depositing $TiO_2$ nanoparticles, $NaGdF_4$:Yb/Tm NPs remained hexagonal. Furthermore, the XRD pattern of Gd-Si and Gd-Si-Ti NPs showed that $SiO_2$ was non-crystalline and $TiO_2$ was anatase structure (JCPDS NO. 21-1272).

The hydrodynamic diameter and surface charge of different nanoparticles were measured by DLS and zeta potential techniques in aqueous solutions. As shown in Fig. 2(b), the sizes of $NaGdF_4$:Yb/Tm, Gd-Si, Gd-Si-Ti and FA-Gd-Si-Ti NPs were 149.7, 204.5, 264.6 and 347.0 nm, respectively. The zeta potentials of $NaGdF_4$:Yb/Tm, Gd-Si, Gd-Si-Ti, $NH_2$-Gd-Si-Ti and FA-Gd-Si-Ti NPs were measured to be 39.4, -25.0, -22.1, 28.5, and 24.1 mV, respectively, as shown in Fig. 2(c). Due to hydroxyl groups exposed on the silica layer and $TiO_2$ crystals, the zeta potentials of Gd-Si and Gd-Si-Ti NPs were negative. After amino modification, the surface charge of $NH_2$-Gd-Si-Ti NPs became positive. From $NH_2$-Gd-Si-Ti NPs to FA-Gd-Si-Ti NPs, the zeta potentials decreased slightly, attributable to partial reaction of amino groups on $NH_2$-Gd-Si-Ti NPs with carboxyl groups from FA molecules.

The UCL spectra of $NaGdF_4$:Yb/Tm, Gd-Si-Ti and FA-Gd-Si-Ti NPs are shown in Fig. 2(d). Under 980 nm laser excitation, the main UCL peaks of $NaGdF_4$:Yb/Tm were located at 362, 452, and 478 nm, attributable to $Tm^{3+}$ transitions of $^1D_2 \rightarrow {}^3H_6$, $^1D_2 \rightarrow {}^3F_4$, and $^1G_4 \rightarrow {}^3H_6$, respectively. Other weak UCL peaks were located at 290, 313, 347, 646, and 692 nm, corresponding

to $^1I_6 \rightarrow ^3H_6$, $^3P_2 \rightarrow ^3F_4$, $^1I_6 \rightarrow ^3F_4$, $^1G_4 \rightarrow ^3F_4$, and $^3F_3 \rightarrow ^3H_6$, respectively. Moreover, the UCL spectra of Gd-Si-Ti and FA-Gd-Si-Ti NPs were similar to that of $NaGdF_4$:Yb/Tm, indicating that $SiO_2$, $TiO_2$ and FA coating did not change the UCL performance of $NaGdF_4$:Yb/Tm. These results also suggested that the as-prepared FA-Gd-Si-Ti NPs could be used as NIR-responsive PDT agents with $TiO_2$ as inorganic photosensitizer.

## 3.2. In Vitro and In Vivo Cytotoxicity of Nanocomposites

The cytotoxicity of the as-prepared nanoparticles was evaluated by MTT assay. Fig. 3

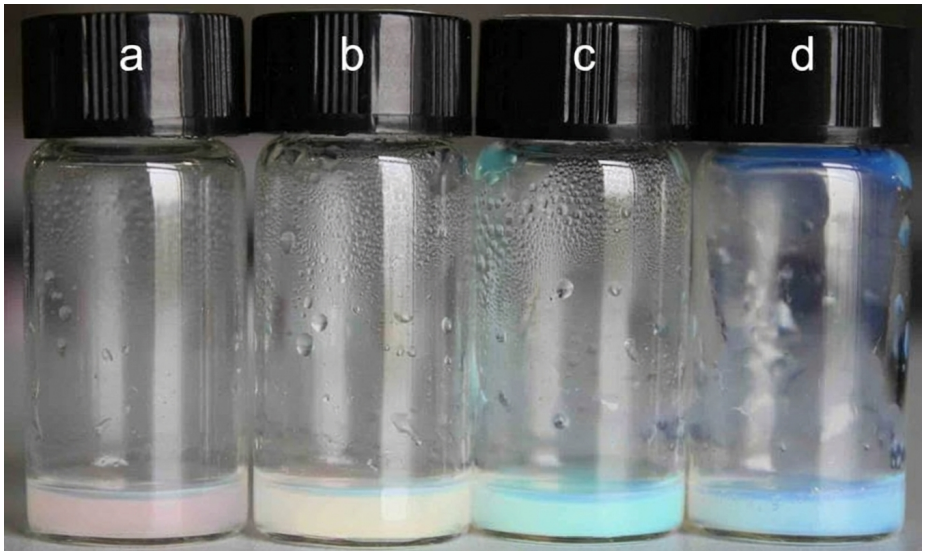


Figure 1: Figure 3

(a) and (c) show the viabilities of HeLa and MCF-7 cells incubated with $NaGdF_4$:Yb/Tm, Gd-Si-Ti and FA-Gd-Si-Ti NPs for 24 h, respectively. At the high concentration of 500 mg/mL, the viabilities of HeLa and MCF-7 cells incubated with FA-Gd-Si-Ti NPs remained above 85% and 89%, respectively, suggesting low cytotoxicity. The cellular location of FA-Gd-Si-Ti NPs was further investigated by bio-TEM analysis. As shown in Fig. 3(b) and (d), numerous FA-Gd-Si-Ti NPs were located in the cytoplasm of HeLa and MCF-7 cells, indicating that FA-targeted Gd-Si-Ti NPs could be effectively taken up and internalized by cancer cells.

To investigate the biocompatibility of FA-Gd-Si-Ti NPs in vivo, healthy nude mice were injected with PBS and FA-Gd-Si-Ti NPs via tail vein, and their major organs were analyzed by H&E staining. Fig. S1 shows H&E staining images of different organs across groups, including heart, liver, spleen, lung, kidney

and intestine. Compared with nude mice treated with PBS only, no noticeable pathological changes such as damage, inflammatory lesions or necrosis were observed in organs of FA-Gd-Si-Ti NPs groups. These results confirmed that the prepared FA-Gd-Si-Ti NPs had good in vivo biocompatibility and potential clinical applicability.

## 3.3. In Vitro and In Vivo MRI Studies

To investigate the MR performance of the as-prepared FA-Gd-Si-Ti NPs, the MR relaxivity of NPs was measured, and MR images of NPs and HeLa and MCF-7 cells incubated with NPs were collected. As shown in Fig. 4 FIGURE:4 and (b), the $r_1$ and $r_2$ values of FA-Gd-Si-Ti NPs were calculated to be 4.53 and 8.82 $mM^{-1}s^{-1}$, respectively. Moreover, the $r_2/r_1$ ratio was about 1.95, which is less than 3, indicating that the as-prepared FA-Gd-Si-Ti NPs had good $T_1$-weighted MR performance. Fig. 4(c) and (d) show the $T_1$- and $T_2$-weighted MR images of FA-Gd-Si-Ti NPs and HeLa and MCF-7 cells incubated with FA-Gd-Si-Ti NPs at different concentrations. $T_1$-weighted MR images of FA-Gd-Si-Ti NPs became brighter with increasing Gd concentrations (from right to left), while $T_2$-weighted MRI images showed little change. Compared with MR images of NPs alone, signals of $T_1$-weighted MR images of HeLa and MCF-7 cells incubated with NPs were weaker due to incomplete NP uptake by cells. The $r_2/r_1$ ratio (1.95) and in vitro MR images indicated that the as-prepared FA-Gd-Si-Ti NPs could serve as potential positive MRI contrast agents.

The in vivo MRI contrast ability of FA-Gd-Si-Ti NPs was also assessed on a 3.0 T clinical MRI instrument. Fig. 5 [FIGURE:5] shows $T_1$ and $T_2$-weighted MR images of MCF-7 tumor-bearing mice before and after intratumoral injection of FA-Gd-Si-Ti NPs. After intratumoral injection of FA-Gd-Si-Ti NPs, the $T_1$-weighted MR image at the tumor site (highlighted with yellow circles) became bright, while the $T_2$-weighted MR image at the tumor site (highlighted with green circles) did not darken, demonstrating that FA-Gd-Si-Ti NPs showed good $T_1$-weighted MRI performance in vivo and have potential for clinical applicability.

## 3.4. In Vitro PDT for MCF-7 and HeLa Cells

Under 980 nm laser irradiation for different durations, the PDT performance of FA-Gd-Si-Ti NPs for HeLa and MCF-7 cells was tested and characterized by MTT assay and CAM/PI staining. As shown in Fig. 6 FIGURE:6 and (b), when irradiation time was 20 min and power density was 0.6 $W/cm^2$, viabilities of HeLa and MCF-7 cells in the control group remained at 92.7% and 91.0%, respectively, indicating negligible killing effect from laser irradiation alone. However, viabilities of HeLa and MCF-7 cells incubated with FA-Gd-Si-Ti NPs decreased to about 35% and 31%, respectively. To monitor PDT effects, HeLa and MCF-7 cells were stained with CAM and PI after different treatments, and fluorescent images were obtained on an inverted fluorescence microscope. As shown in Fig.

6(c) and (d), when HeLa and MCF-7 cells were only incubated with FA-Gd-Si-Ti NPs or only irradiated by 980 nm laser for 20 min, only some cells were stained red. However, when cells were incubated with FA-Gd-Si-Ti NPs and irradiated by 980 nm laser for 20 min, more than 65% of cells were stained red. These staining results were consistent with MTT data shown in Fig. 6(a) and (b).

Furthermore, under 980 nm laser irradiation, the viability of HeLa and MCF-7 cells incubated with only 234 mg/mL $NaGdF_4$:Yb/Tm NPs (equivalent concentration of $NaGdF_4$:Yb/Tm in 500 mg/mL FA-Gd-Si-Ti NPs) was also measured, with the same irradiation time and power density as in Fig. 6. Viabilities of HeLa and MCF-7 cells only decreased to about 68.2% and 73.8%, respectively, as shown in Fig. S2(a) and (b). Similarly, in Fig. S2(c) and (d), only a few HeLa and MCF-7 cells were stained red after incubation with $NaGdF_4$:Yb/Tm NPs and 980 nm laser irradiation, consistent with MTT results in Fig. S2(a) and (b).

Comparing Fig. 6 and Fig. S2, the PDT effect arose from two factors: reactive oxygen from $TiO_2$ nanoparticles and UV light from UCL of $NaGdF_4$:Yb/Tm NPs. Moreover, $TiO_2$ nanoparticles played a more important role in killing cancer cells. These results also suggested that NIR-responsive PDT of $TiO_2$ nanoparticles could be achieved and improved by coupling UCL NPs with $TiO_2$ NPs.

## 3.5. In Vivo PDT for MCF-7 Tumor-Bearing Nude Mice

MCF-7 tumor-bearing nude mice in four experimental groups were used to investigate in vivo PDT performance of FA-Gd-Si-Ti NPs under 980 nm laser irradiation via intratumoral injection with different materials. As shown in Fig. 7 FIGURE:7, relative tumor volumes increased from 1 to 2.7, 2.5, and 2.3 in PBS, FA-Gd-Si-Ti NPs, and PBS + NIR irradiation groups after 2-week treatment. However, in the FA-Gd-Si-Ti NPs + NIR irradiation group, tumor volume decreased to about 0.3, with a growth inhibition ratio of about 88.6% after 2-week treatment. These results suggested that FA-Gd-Si-Ti NPs with 980 nm irradiation have excellent therapeutic effect in inhibiting tumor growth. Fig. 7(b) shows the body weight change trend across groups during 2-week treatment. Body weight of tumor-bearing nude mice in all groups did not change significantly, implying minimal systemic toxicity.

PDT efficiency was also evaluated by H&E staining of tumor tissue sections. As shown in Fig. 7(c), extensive coagulative necrosis was observed in histological sections of the FA-Gd-Si-Ti NPs + NIR group, indicating that tumor cells were destroyed by PDT under 980 nm laser irradiation. However, in other experimental groups (PBS, FA-Gd-Si-Ti NPs, and PBS + NIR irradiation), large areas of neoplastic cells with nuclear atypia were observed in tumor histological sections, suggesting insufficient tumor damage. The in vivo PDT results revealed that FA-Gd-Si-Ti NPs have potential clinical applicability as NIR-responsive PDT

agents.

Histological analysis of heart, liver, spleen, lung, and kidney in different groups was also performed by H&E staining after 2-week treatment. As shown in Fig. 8 [FIGURE:8], no pathological changes or necrosis were found in these major organs across groups. Fibrosis in heart and lung samples was not detected, and inflammatory reaction in liver sections was also absent. Moreover, glomerular and tubular structures in kidney samples were clearly displayed. These results demonstrated the safety of FA-Gd-Si-Ti NPs and their potential clinical application for MRI and NIR-responsive PDT of cancers.

In past decades, $TiO_2$ inorganic photosensitizer was reported for UV-responsive PDT of cancers, and in this work NIR-responsive PDT of $TiO_2$ inorganic photosensitizer was investigated by coupling UCL NPs that convert NIR to UV light. However, the PDT mechanism of $TiO_2$ nanoparticles is more complicated compared with organic photosensitizers. Different reactive oxygen radicals such as $OH\cdot$, $O_2^-$, $H_2O_2$ and $^1O_2$ are induced by triggering $TiO_2$ under UV light, but it remains unclear which radicals play the leading role in PDT. Exploring the PDT mechanism of $TiO_2$ nanoparticles remains a great challenge that should be deeply investigated in the future.

## 4. Conclusions

$TiO_2$ inorganic photosensitizer coupled Gd-based UCL ($NaGdF_4$:Yb/Tm@$SiO_2$@TiO$_{2}$)*nanocompositesw*
*responsivePDTofcancers*, *whereinTiO*_{2}$ could be excited by 980 nm laser due to UCL of $NaGdF_4$:Yb/Tm converting NIR to UV light. The cytotoxicity, MRI and PDT of FA-Gd-Si-Ti NPs in vitro and in vivo were systematically investigated. The results showed that the as-prepared FA-Gd-Si-Ti NPs had good biocompatibility, and MR relaxivity measurement demonstrated that FA-Gd-Si-Ti NPs were effective $T_1$-weighted MRI contrast agents with high $r_1$ relaxivity of 4.53 $mM^{-1}s^{-1}$. Under 980 nm laser irradiation, in vitro PDT of FA-Gd-Si-Ti NPs showed that 65–70% of cells could be killed, with both reactive oxygen from $TiO_2$ inorganic photosensitizer and UV light from UCL contributing, though reactive oxygen from $TiO_2$ played the more important role. Furthermore, in vivo PDT of MCF-7 tumor-bearing mice revealed a tumor inhibition ratio of up to about 88.6% after 2-week treatment. As a result, FA-targeted $NaGdF_4$:Yb/Tm@$SiO_2$@TiO$_{2}$ nanocomposites have potential applications in both MRI and NIR-responsive inorganic PDT of cancers in deep tissues.

## Acknowledgments

This work was supported by the National Natural Science Foundation of China (U1332117, U1432114), the National Key Basic Research Program of China (2014CB744504), the Postdoctoral Science Foundation of China and Jiangsu Province, and the Hundred Talents Program of Chinese Academy of Sciences.

## Appendix A. Supplementary Data

Supplementary data related to this article can be found at http://dx.doi.org/10.1016/j.biomaterials.2014.12.040.

## References

[1] Bonnett R. Photosensitizers of the porphyrin and phthalocyanine series for photodynamic therapy. Chem Soc Rev 1995;24:19–33.
[2] Dolmans DEJGJ, Fukumura D, Jain RK. Photodynamic therapy for cancer. Nat Rev Cancer 2003;3:380–7.
[3] Gu H, Xu K, Yang Z, Chang CK, Xu B. Synthesis and cellular uptake of porphyrin decorated iron oxide nanoparticles—a potential candidate for bimodal anti-cancer therapy. Chem Commun 2005:4270–2.
[4] Cheng Y, Samia AC, Meyers JD, Panagopoulos I, Fei B, Burda C. Highly efficient drug delivery with gold nanoparticle vectors for in vivo photodynamic therapy of cancer. J Am Chem Soc 2008;130:10643–7.
[5] Moan J. Effect of bleaching of porphyrin sensitizers during photodynamic therapy. Cancer Lett 1986;33:45–53.
[6] Stummer W, Pichlmeier U, Meinel T, Wiestler OD, Zanella F, Reulen HJ. Fluorescence-guided surgery with 5-aminolevulinic acid for resection of malignant glioma: a randomised controlled multicentre phase III trial. Lancet Oncol 2006;7:392–401.
[7] Zhao T, Wu H, Yao SQ, Xu Q-H, Xu GQ. Nanocomposites containing gold nanorods and porphyrin-doped mesoporous silica with dual capability of two-photon imaging and photosensitization. Langmuir 2010;26:14937–42.
[8] Xia L, Kong X, Liu X, Tu L, Zhang Y, Chang Y, et al. An upconversion nanoparticle–zinc phthalocyanine based nanophotosensitizer for photodynamic therapy. Biomaterials 2014;35:4146–56.
[9] Park YI, Kim HM, Kim JH, Moon KC, Yoo B, Lee KT, et al. Theranostic probe based on lanthanide-doped nanoparticles for simultaneous in vivo dual-modal imaging and photodynamic therapy. Adv Mater 2012;24:5755–61.
[10] Jin S, Zhou L, Gu Z, Tian G, Yan L, Ren W, et al. A new near infrared photosensitizing nanoplatform containing blue-emitting up-conversion nanoparticles and hypocrellin A for photodynamic therapy of cancer cells. Nanoscale 2013;5:11910–8.
[11] Qiao XF, Zhou JC, Xiao JW, Wang YF, Sun LD, Yan CH. Triple-functional core-shell structured upconversion luminescent nanoparticles covalently grafted with photosensitizer for luminescent, magnetic resonance imaging and photodynamic therapy in vitro. Nanoscale 2012;4:4611–23.
[12] Zhao Z, Han Y, Lin C, Hu D, Wang F, Chen X, et al. Multifunctional core–shell upconverting nanoparticles for imaging and photodynamic therapy of liver cancer cells. Chem Asian J 2012;7:830–7.
[13] Allison RR, Downie GH, Cuenca R, Hu XH, Childs CJH, Sibata CH. Photosensitizers in clinical PDT. Photodiagn Photodyn 2004;1:27–42.
[14] Qian HS, Guo HC, Ho PC, Mahendran R, Zhang Y. Mesoporous-silica-coated up-conversion fluorescent nanoparticles for photodynamic therapy.

Small 2009;5:2285–90.
[15] Linsebigler AL, Lu G, Yates JT. Photocatalysis on $TiO_2$ surfaces: principles, mechanisms, and selected results. Chem Rev 1995;95:735–58.
[16] Ohko Y, Tryk DA, Hashimoto K, Fujishima A. Autoxidation of acetaldehyde initiated by $TiO_2$ photocatalysis under weak UV illumination. J Phys Chem B 1998;102:2699–704.
[17] Wang W, Huang W, Ni Y, Lu C, Xu Z. Different upconversion properties of $\beta$-$NaYF_4$:$Yb^{3+}$,$Tm^{3+}$/$Er^{3+}$ in affecting the near-infrared-driven photocatalytic activity of high-reactive $TiO_2$. ACS Appl Mater Interf 2013;6:340–8.
[18] Xu D-X, Lian Z-W, Fu M-L, Yuan B, Shi J-W, Cui H-J. Advanced near-infrared-driven photocatalyst: fabrication, characterization, and photocatalytic performance of $\beta$-$NaYF_4$:$Yb^{3+}$,$Tm^{3+}$@TiO$_{2}$ core@shell microcrystals. Appl Catal B-Environ 2013;142–143:377–86.
[19] Zhang Y, Hong Z. Synthesis of lanthanide-doped $NaYF_4$@TiO$_{2}$ core-shell composites with highly crystalline and tunable $TiO_2$ shells under mild conditions and their upconversion-based photocatalysis. Nanoscale 2013;5:8930–3.
[20] Paunesku T, Rajh T, Wiederrecht G, Maser J, Vogt S, Stojicevic N, et al. Biology of $TiO_2$-oligonucleotide nanocomposites. Nat Mater 2003;2:343–6.
[21] Rozhkova EA, Ulasov I, Lai B, Dimitrijevic NM, Lesniak MS, Rajh T. A high-performance nanobio photocatalyst for targeted brain cancer therapy. Nano Lett 2009;9:3337–42.
[22] Seo JW, Chung H, Kim MY, Lee J, Choi IH, Cheon J. Development of water-soluble single-crystalline $TiO_2$ nanoparticles for photocatalytic cancer-cell treatment. Small 2007;3:850–3.
[23] Yamaguchi S, Kobayashi H, Narita T, Kanehira K, Sonezaki S, Kubota Y, et al. Novel photodynamic therapy using water-dispersed $TiO_2$-polyethylene glycol compound: evaluation of antitumor effect on glioma cells and spheroids in vitro. Photochem Photobiol 2010;86:964–71.
[24] Higuchi Y. Chromosomal DNA fragmentation in apoptosis and necrosis induced by oxidative stress. Biochem Pharmacol 2003;66:1527–35.
[25] Zeng L, Ren W, Xiang L, Zheng J, Chen B, Wu A. Multifunctional $Fe_3O_4$-$TiO_2$ nanocomposites for magnetic resonance imaging and potential photodynamic therapy. Nanoscale 2013;5:2107–13.
[26] Liu K, Wang Y, Kong X, Liu X, Zhang Y, Tu L, et al. Multispectral upconversion luminescence intensity ratios for ascertaining the tissue imaging depth. Nanoscale 2014;6:9257–63.
[27] Xu CT, Svensson N, Axelsson J, Svenmarker P, Somesfalean G, Chen G, et al. Autofluorescence insensitive imaging using upconverting nanocrystals in scattering media. Appl Phys Lett 2008;93:171103–171103-3.
[28] He M, Huang P, Zhang C, Hu H, Bao C, Gao G, et al. Dual phase-controlled synthesis of uniform lanthanide-doped $NaGdF_4$ upconversion nanocrystals via an OA/ionic liquid two-phase system for in vivo dual-modality imaging. Adv Funct Mater 2011;21:4470–7.
[29] Wang F, Han Y, Lim CS, Lu Y, Wang J, Xu J, et al. Simultaneous phase and size control of upconversion nanocrystals through lanthanide doping.

Nature 2010;463:1061–5.
[30] Wang F, Wang J, Liu X. Direct evidence of a surface quenching effect on size-dependent luminescence of upconversion nanoparticles. Angew Chem Int Ed 2010;122:7618–22.
[31] Chen F, Bu W, Zhang S, Liu J, Fan W, Zhou L, et al. $Gd^{3+}$-ion-doped upconversion nanoprobes: relaxivity mechanism probing and sensitivity optimization. Adv Funct Mater 2013;23:298–307.
[32] Hou Y, Qiao R, Fang F, Wang X, Dong C, Liu K, et al. $NaGdF_4$ nanoparticle-based molecular probes for magnetic resonance imaging of intraperitoneal tumor xenografts in vivo. ACS Nano 2012;7:330–8.
[33] Johnson NJJ, Oakden W, Stanisz GJ, Scott Prosser R, van Veggel FCJM. Size-tunable, ultrasmall $NaGdF_4$ nanoparticles: insights into their $T_1$ MRI contrast enhancement. Chem Mater 2011;23:3714–22.
[34] Liu F, He X, Liu L, You H, Zhang H, Wang Z. Conjugation of $NaGdF_4$ upconverting nanoparticles on silica nanospheres as contrast agents for multimodality imaging. Biomaterials 2013;34:5218–25.
[35] Na HB, Song IC, Hyeon T. Inorganic nanoparticles for MRI contrast agents. Adv Mater 2009;21:2133–48.
[36] Zhang D, Zhao D, Zheng K, Liu N, Qin W. Synthesis and upconversion luminescence of $NaYF_4$:Yb, Tm/$TiO_2$ core/shell nanoparticles with controllable shell thickness. J Nanosci Nanotechno 2011;11:9761–4.